

ON A GIANT IMPACT ORIGIN OF CHARON, NIX, AND HYDRA

ROBIN M. CANUP

Planetary Science Directorate, Southwest Research Institute, 1050 Walnut Street, Suite 300, Boulder, CO 80302, USA; robin@boulder.swri.edu
Received 2010 August 13; accepted 2010 November 29; published 2010 December 29

ABSTRACT

It is generally believed that Charon was formed as a result of a large, grazing collision with Pluto that supplied the Pluto–Charon system with its high angular momentum. It has also been proposed that Pluto’s small outer moons, Nix and Hydra, formed from debris from the Charon-forming impact, although the viability of this scenario remains unclear. Here I use smooth particle hydrodynamics impact simulations to show that it is possible to simultaneously form an intact Charon and an accompanying debris disk from a single impact. The successful cases involve colliding objects that are partially differentiated prior to impact, having thin outer ice mantles overlying a uniform composition rock–ice core. The composition of the resulting debris disks varies from a mixture of rock and ice (similar to the bulk composition of Pluto and Charon) to a pure ice disk. If Nix and Hydra were formed from such an impact-generated disk, their densities should be less than or similar to that of Charon and Pluto, and the small moons could be composed entirely of ice. If they were instead formed from captured material, a mixed rock–ice composition and densities similar to that of Charon and Pluto would be expected. Improved constraints on the properties of Nix and Hydra through occultations and/or the *New Horizons* encounter may thus help to distinguish between these two modes of origin, particularly if the small moons are found to have ice-like densities.

Key words: Kuiper belt: general – Kuiper belt objects: individual (Pluto) – planets and satellites: formation

1. BACKGROUND

Pluto and its massive satellite, Charon, are thought to have formed as a result of a giant impact (McKinnon 1989; Canup 2005), in an event similar to that believed responsible for the origin of Earth’s Moon (Canup & Asphaug 2001; Canup 2004, 2008). It has been suggested that the satellites of other large Kuiper Belt objects are also products of large collisions (e.g., Brown et al. 2006). In this paper, I explore whether the two much smaller, and more recently discovered, outer satellites of Pluto—Nix and Hydra—could have been byproducts of the same collision that produced Charon, and characterize the potentially observable characteristics of such an impact-produced multiple satellite system.

1.1. Formation of the Pluto–Charon System by Impact

The radii, masses, and mean densities of Pluto and Charon remain somewhat uncertain. Recent values from Tholen et al. (2008, and references therein) are shown in Table 1. The mass ratio of Charon to Pluto, q , is estimated to be $q = 0.1166 \pm 0.0069$ (Tholen et al. 2008). Estimated densities for Pluto and Charon imply rock–ice compositions with approximately 50%–80% rock by mass (e.g., Olkin et al. 2003). The angular momentum of the Pluto–Charon system is approximately $L_{PC} \approx q\omega M_{PC}a^2/(1+q)^2$ (e.g., Canup 2005), where ω is the angular velocity corresponding to the observed orbital period of 6.387 days, a is Charon’s semimajor axis, and I have neglected the small, several percent contribution to L_{PC} due to the spins of Pluto and Charon. For a total system mass $M_{PC} = 1.456 \times 10^{25}$ g, $q = 0.117$, and $a = 19,570$ km, the system angular momentum is $L_{PC} \approx 6.0 \times 10^{37}$ g cm² s⁻¹. Scaling this by the quantity $L' \equiv \sqrt{GM_{PC}^3 R_{PC}}$ (where R_{PC} is the radius of an equivalent spherical object containing a mass M_{PC} and having a density equal to the mean density of the Pluto–Charon pair, $\langle \rho \rangle \approx 2$ g cm⁻³) gives a normalized system angular momentum, $J_{PC} \equiv L_{PC}/L'$, of $J_{PC} \approx 0.38$.

Canup (2005) presented results of 120 smooth particle hydrodynamics (SPH) simulations of potential Pluto–Charon-forming impacts. The simulations considered a range of impactor and target masses and compositions, impact velocities, pre-impact spin states, and impact angles. Two types of impacts were identified as capable of producing a satellite as massive as Charon (i.e., having $q \geq 0.1$). In the first, a grazing, low-velocity collision involving similarly sized, differentiated objects (with ice mantles and rock or rock–metal cores, containing 40%–50% ice by mass) produces an orbiting disk of ice, with the rocky cores of both of the colliding objects absorbed by the final planet. The disk produced by this type of collision (shown in Canup 2005, Figure 1) could then later accumulate into a satellite, which would be predominantly icy with a density substantially lower than that of the planet. A similar “graze and merge” collision between objects containing ~20%–25% ice by mass has recently been advocated for the origin of Haumea and its ice-rich collisional family (Leinhardt et al. 2010). However in the case of the Pluto–Charon system, both Charon’s sizable rock fraction and its large mass relative to Pluto are rather difficult to explain through a graze and merge scenario (Canup 2005).

Canup (2005) instead advocated a second class of impact, involving an oblique, low-velocity collision by a uniform composition, undifferentiated impactor containing $\geq 0.3M_{PC}$. With an undifferentiated impactor, the binary can form directly as a result of the collision, with the satellite arising from an intact portion of the impactor (shown in Canup 2005, Figure 2). The final satellite’s composition is similar to that of the impactor (i.e., a mixture of rock and ice), and the satellite’s initial orbit is quite eccentric ($0.1 < e < 0.8$) with a semimajor axis typically between ~ 3 and $15R_p$ and a periape between ~ 2.5 and $4R_p$, where R_p is the radius of the final planet. Several dozen cases displaying this behavior produced binary pairs with $0.03 < q < 0.36$ and $0.3 \leq J \leq 0.5$ (Canup 2005). The planet’s rapid post-impact rotation leads to an initial co-rotation radius that is typically interior to $2R_p$, so that tides raised on the planet by the satellite would transfer angular momentum to

Table 1
Estimated Properties of the Pluto System^a

Object	Radius (km)	Mass (g)	Density (g cm ⁻³)	Semimajor Axis (in Pluto Radii)
Pluto	[1147]	1.30×10^{25}	2.06	...
Charon	606	1.52×10^{24}	1.63	17
Nix	44	5.8×10^{20}	[1.63]	43
Hydra	36	3.2×10^{20}	[1.63]	57

Note. ^a Values shown are from Tholen et al. (2008); square brackets indicate assumed quantities.

the satellite’s orbit. Charon’s current orbit has $a \approx 17R_P$ and the Pluto–Charon binary is in the dual synchronous state, in which the length of Pluto’s day equals both Charon’s orbital period and Charon’s day (e.g., Dobrovolskis et al. 1997).

1.2. Nix and Hydra

Hubble Space Telescope observations in 2005 May (Weaver et al. 2006) detected two satellites orbiting Pluto exterior to Charon; subsequent to these findings, the satellites were also detected in data from earlier observations (Buie et al. 2006). Charon and the small satellites display nearly a 12:3:2 orbital frequency relationship, with Nix and Hydra being located near the 4:1 and 6:1 mean-motion commensurabilities with Charon and near the 3:2 commensurability with one another. The outer satellites are quite small, having estimated radii of about 40 km and masses $\sim \text{few} \times 10^{20}$ g (see Table 1 and Tholen et al. 2008). These masses are more than three orders of magnitude smaller than Charon’s mass (1.5×10^{24} g). Charon, Nix, and Hydra are nearly co-planar, orbit in the same sense as Pluto’s rotation, and have nearly circular orbits (e.g., Tholen et al. 2008). All three satellite orbits are extremely compact compared to the maximum possible orbital radius at which a satellite could remain bound to Pluto, which is comparable to Pluto’s Hill radius, $R_{\text{Hill}} = a_P[(M_{\text{PC}})/3M_{\text{Sun}}]^{1/3} \sim 7 \times 10^3 R_P$, where a_P is Pluto’s semimajor axis, M_{Sun} is the Sun’s mass, and R_P is Pluto’s radius.

Obvious candidate mechanisms for forming Nix and Hydra include formation via impact or by capture. Origin of all three satellites from an impact-generated disk would naturally account for their prograde (with respect to Pluto’s rotation) and nearly co-planar orbits. In addition, a large impact appears necessary to produce Charon and the high Pluto–Charon system angular momentum. Intact capture of the smaller satellites would not generally select for a preferred orbital direction and would tend to produce higher eccentricity and inclination orbits, such as those seen in the irregular satellites of the giant planets (e.g., Nicholson et al. 2008). Thus given the basic properties of the Pluto–Charon–Nix–Hydra system, an impact origin for all three satellites appears more likely (e.g., Stern et al. 2006).

The current orbital radii of Nix and Hydra are, however, larger than those of bound debris produced by typical satellite-forming impacts (e.g., Canup 2004). The new satellites could not have achieved their current distances through direct tidal interactions with Pluto, given their small masses and large orbital radii. It has been proposed that Nix and Hydra were trapped in 4:1 and 6:1 co-rotation resonances with the young, eccentricly orbiting Charon, so that the outer small satellites were driven outward as Charon’s orbit expanded due to its tidal interaction with Pluto (Ward & Canup 2006). In this way, Nix and Hydra could have formed in more compact orbits: the 4:1 and 6:1 resonances are located at approximately $(4)^{2/3}a$ and $(6)^{2/3}a$, respectively, or, e.g., at ~ 13 and $17R_P$ for an early Charon with $a = 5R_P$. Subsequent works argue that the co-rotation

resonance scenario can operate for Nix or Hydra, but not both (Lithwick & Wu 2008), or that it might allow both satellites to be resonantly transported for only a limited range of conditions (Ward & Canup 2010). Other resonance solutions may exist (e.g., Lithwick & Wu 2010), but at this time a complete model of the resonant expansion of Nix and Hydra by Charon remains elusive (e.g., Peale et al. 2010).

A second open issue with an impact origin of Nix and Hydra is that none of the prior impact simulations that produced an intact Charon left debris in orbits exterior to Charon. However, the simulations in Canup (2005) considered a limited range of impactor and target compositions and did not have sufficiently high numerical resolution to track the small masses of Nix or Hydra. In this paper, I use high-resolution SPH simulations to assess (1) whether an impact that produces the Pluto–Charon pair can also leave a debris disk from which additional small satellites could later accrete, and (2) the potentially observable consequences of such an event.

2. METHOD

The simulations here and in Canup (2005) utilize SPH (e.g., Benz 1989, from whose work my code is directly descended; see also Canup & Asphaug 2001 and Canup 2004). SPH is a Lagrangian method that is well suited for modeling large collisions in which matter undergoes deformation and substantial spatial dispersal. In SPH, colliding objects are represented by a multitude of spherical overlapping “particles”. Each particle represents a quantity of mass of a given composition, whose three-dimensional spatial extent is specified by a probability density function, the kernel, and the characteristic width of the particle, the smoothing length. For the gravity-regime impacts of interest here material strength is ignored, and the evolution of each particle’s kinematic (position and velocity) and state (internal energy, density) variables are evolved due to (1) explicit gravitational interaction with all other particles, (2) compressional heating and expansional cooling, and (3) shock dissipation. The specified equation of state then returns a pressure as a function of internal energy, u , and density, ρ . Chemical interaction between particles of different compositions or mixing at a scale smaller than an individual SPH particle are not treated.

I utilize the M-ANEOS equation of state (Melosh 2007), using the same material parameters as in Canup (2005; see also Canup & Pierazzo 2006). ANEOS (Thompson & Lauson 1972) is a semi-analytical equation of state that uses an interpolation function to calculate the Helmholtz free energy given an input ρ and temperature, with the latter determined by an initial iteration given ρ and u . ANEOS accounts for phase changes and can include different phases (e.g., liquid and vapor) within a single SPH particle under the assumption that the phases are in temperature and pressure equilibrium.

This work utilizes a new, parallelized version of SPH that allows for greater numbers of particles and therefore finer spatial

and mass resolution. Most of the simulations in Canup (2005) involved a total of $N = 2 \times 10^4$ particles, so that each particle contained $\sim 10^{21}$ g and the masses of Nix and Hydra ($\sim \text{few} \times 10^{20}$ g) were not resolved. Here I use $N = 10^5$ – 10^6 particles per collision, so that each SPH particle contains $\sim 10^{19}$ – 10^{20} g. Even with the parallelized code, the million-particle simulations are computationally intensive: each 10^6 -particle simulation required several months on a dedicated eight-node cluster. Increasing N slows the calculation in two ways: (1) the number of gravitational force and nearest neighbor calculations that must be performed at each time step is increased, and (2) the time step needed to satisfy the Courant condition (which requires that the time step be smaller than the sound speed crossing time across the smallest SPH particle) is reduced as the spatial resolution is increased.

The colliding objects are generated with an initially uniform spacing between the SPH particles. They are then simulated in isolation for about 10 hr, allowing them to settle to a hydrostatically equilibrated state prior to the collision.

3. IMPACT SIMULATION RESULTS

3.1. Uniform Composition Impactor + Target

Figure 1 shows a million-particle simulation of the grazing collision of two undifferentiated objects (both composed of pure serpentine, a representative hydrated silicate) in a collision similar to the intact moon cases identified in Canup (2005), specifically the one shown in Figure 2 of that paper. The impactor-to-total mass ratio is $\gamma = 0.3$, the impact speed is equal to the mutual escape velocity ($v_{\text{imp}} = v_{\text{esc}} = \sqrt{2GM_T/(R_{\text{imp}} + R_{\text{tar}})}$, where M_T is the total colliding mass, and R_{imp} and R_{tar} are the impactor and target radii), the total mass is $M_T = 1.46 \times 10^{25}$ g, the colliding objects have no pre-impact spin, the total angular momentum is $L_T = 5.4 \times 10^{37}$ g cm² s⁻¹, the scaled angular momentum is $J = 0.35$ (where R_{PC} is computed assuming an average density appropriate for serpentine objects, 2.5 g cm⁻³), and the scaled impact parameter is $b = 0.96$ (with $b \equiv \sin \xi$, where ξ is the impact angle and $b = 1$ for a grazing impact). The results of this simulation are broadly similar to those found in Canup (2005). Here the final satellite-to-planet mass ratio is $q = 0.10$, and the satellite's orbital eccentricity is $e = 0.8$ and its semimajor axis is $a = 16.9R_p$. At the end of the simulation, there is some orbiting debris separate from satellite (a total mass of $\sim 10^{22}$ g), but its proximity to the large satellite suggests that it will be accumulated by the satellite and will not form a stable separate moon.

Thus for the collision of uniform composition/undifferentiated objects, increasing the number of SPH particles by a factor of 50 produces a comparable result to that found in Canup (2005) with lower resolution simulations: a binary planet–moon system without a debris disk. Such a collision would not naturally yield exterior small moons.

3.2. Partially Differentiated Impactor + Target

Because of the differences in material properties between ice and rock (notably ice's lower density, vaporization temperature, and latent heat of vaporization), the behavior of these materials can differ in a large collision. Canup (2005) found that the collision of similarly sized, half-ice/half-rock objects that are fully differentiated produces a disk (rather than an intact moon), and that the disk is composed overwhelmingly of ice, with the higher density components accumulated by the planet's core.

The disks produced by these types of impacts tend to contain too little mass to account for Charon except in rather extreme cases (see supporting online material in Canup 2005), and would yield a satellite that is primarily composed of ice, in contrast to the mixture of rock and ice implied by Charon's density.

Here I consider an alternative initial composition intended to mimic a partially differentiated state, in which the colliding objects are predominantly uniform composition ($\sim 90\%$ serpentine by mass) with a small fraction of their mass contained in a thin outer pure ice shell ($\sim 10\%$ by mass). Temperatures in the initial, pre-collision ice shell are set to ~ 200 – 240 K intended to represent conditions in an early large Kuiper Belt object.

Figures 2 and 3 show a million-particle simulation of a collision with $\gamma = 0.3$, $v_{\text{imp}} = v_{\text{esc}}$, $M_T = 1.46 \times 10^{25}$ g, $b = 0.94$, $L_T = 5.4 \times 10^{37}$ g cm² s⁻¹, $J = 0.35$ (where R_{PC} is here computed for an average density of 2.2 g cm⁻³), and no pre-impact spin in the impactor or target. This is similar to the collision shown in Figure 1, only here the colliding objects are partially differentiated with 10% ice by mass. While the overall behavior is similar to that in Figure 1, the intact moon is accompanied by a dispersed disk of material originating primarily from the icy mantles of both objects. The disk (defined as those particles not in either the planet or the moon with $v^2/2 < GM_T/r$, where v and r are the particle's velocity and position in the center-of-mass frame, and M_T is the total mass in the planet and the moon) contains 6×10^{21} g. Approximately 3×10^{21} g escapes the system altogether. The intact moon's orbit has $e = 0.5$ and $a = 7.3R_p$, and it is somewhat less massive than the case shown in Figure 1 ($q = 0.08$ versus $q = 0.1$).

A third million-particle simulation considered the collision of partially differentiated objects with $\gamma = 0.3$, $v_{\text{imp}} = 1.1v_{\text{esc}}$, $M_T = 1.46 \times 10^{25}$ g, $L_T = 5.3 \times 10^{37}$ g cm² s⁻¹, $J = 0.34$, a scaled impact parameter of $b = 0.82$, and an impactor with a 7 hr spin period prior to the impact that was prograde with respect to the direction of the impact (with the pre-impact spin axis aligned with the impact angular momentum vector, as in Canup 2005). The overall evolution was similar to that shown in Figures 2 and 3, with a final intact moon having $q = 0.07$, $e = 0.4$, and $a = 6.7R_p$, accompanied by a predominantly ice disk containing 8×10^{21} g, with $\sim 10^{22}$ g escaping. Figure 4(a) shows a mapping of the final predicted state (escaping, orbiting the planet, or accreted by the central planet) of each SPH particle from this simulation onto the figures of the original objects. Here a particle is defined as orbiting the planet if it has a negative energy in the center-of-mass frame, and its equivalent circular orbital radius, a_{eq} , is above the surface of the planet, where a_{eq} is defined as the circular orbit containing the same total angular momentum as the component of the particle's angular momentum in the center-of-mass frame that is normal to the plane of the impact (as in Canup 2004). Figure 4(b) shows a similar mapping of the peak temperature experienced by each particle during the impact for comparison. The highest shock pressures and temperature increases due to the impact are generated at the initial impact interface. Much of the most highly heated ice dynamically escapes the system (red particles in Figure 4(a)), while some ends up in the dispersed ice disk. The intact moon originates from the large, contiguous region of yellow–green particles in the upper left portion of the impactor in Figure 4(a).

To more fully explore the relevant parameter space, I completed a series of about 30 10^5 -particle simulations that considered $M_T = M_{\text{PC}}$, $\gamma = 0.3$ and 0.5 , $1 \leq v_{\text{imp}}/v_{\text{esc}} \leq 1.4$,

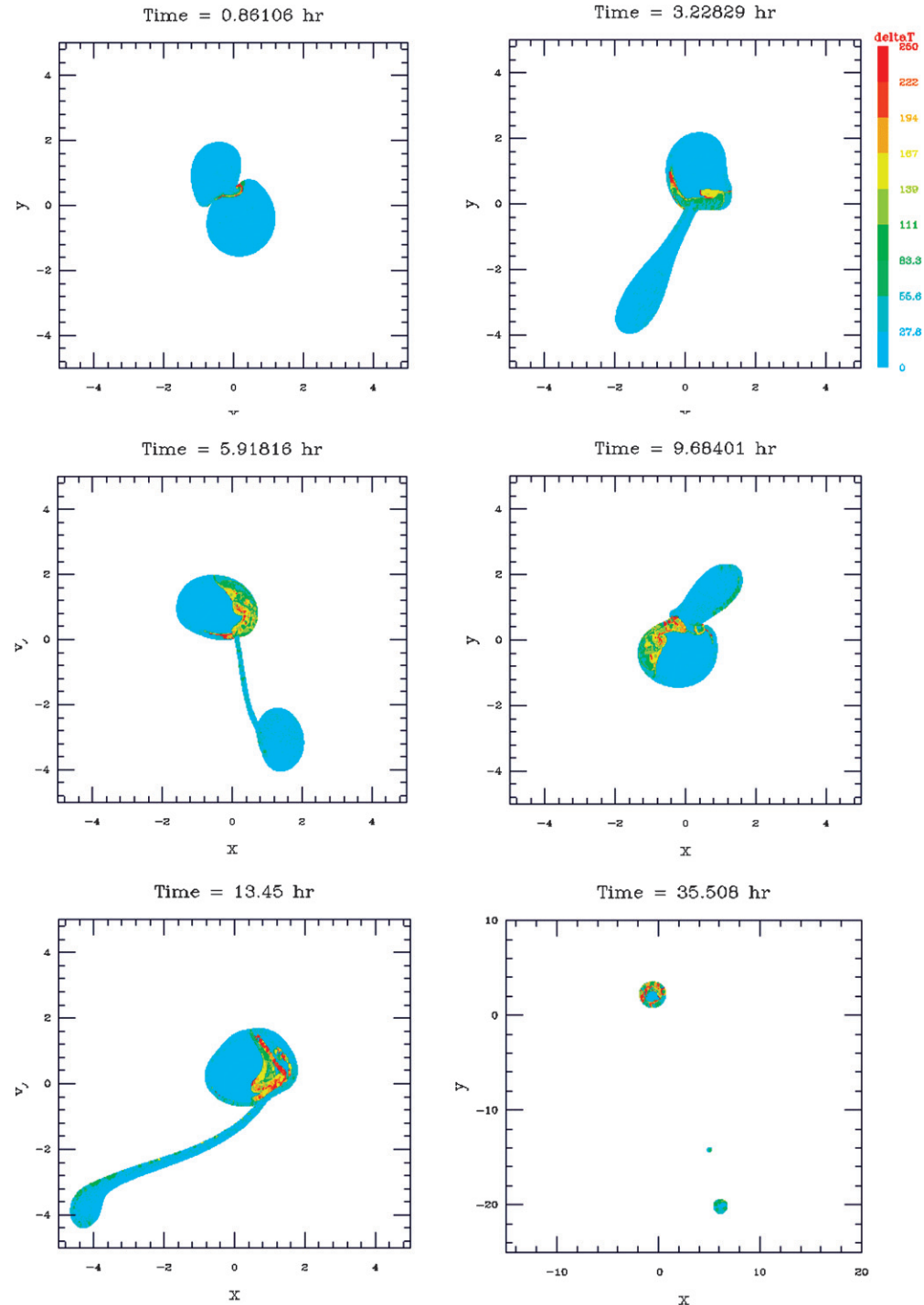


Figure 1. Grazing collision of two undifferentiated, uniform-composition objects produces a Pluto–Charon-type binary. Color scales with the temperature change at each time relative to values at the start of the simulation; distances are shown in units of 10^3 km. This collision is similar to that shown in Figure 2 of Canup (2005), only here performed with a factor of 50 more SPH particles (a total of 10^6 particles). The final large satellite (bottom right panel) contains 10% of the planet’s mass and is accompanied by a much smaller clump of particles orbiting nearby. The lack of an extended debris disk makes this collision a poor candidate for forming small satellites exterior to Charon.

$0.75 \leq b \leq 0.98$, and several pre-impact prograde spin states in the impactor (no spin, 3 hr prograde spin, and 5 hr prograde spin). The impact conditions were chosen to yield a scaled total angular momentum (including both the angular momentum due to the collision and that due to any pre-impact rotation in the impactor) in the range $0.34 \leq J \leq 0.46$, bracketing the estimated value for the Pluto–Charon system ($J \approx 0.38$). The pre-collision objects were partially differentiated, containing 15% of their

mass in a pure ice outer shell and the remainder in a uniform composition, serpentine interior.

Three basic outcomes resulted: (1) formation of a large intact moon and a debris disk (similar to the 10^6 -particle simulations shown in Figures 2–4); (2) formation of a mixed ice–rock disk with a total mass much less than that of Charon; and (3) escape of the impactor. Table 2 shows the occurrence of these outcomes as a function of the γ , v_{imp} , b , and J values of each simulation. In

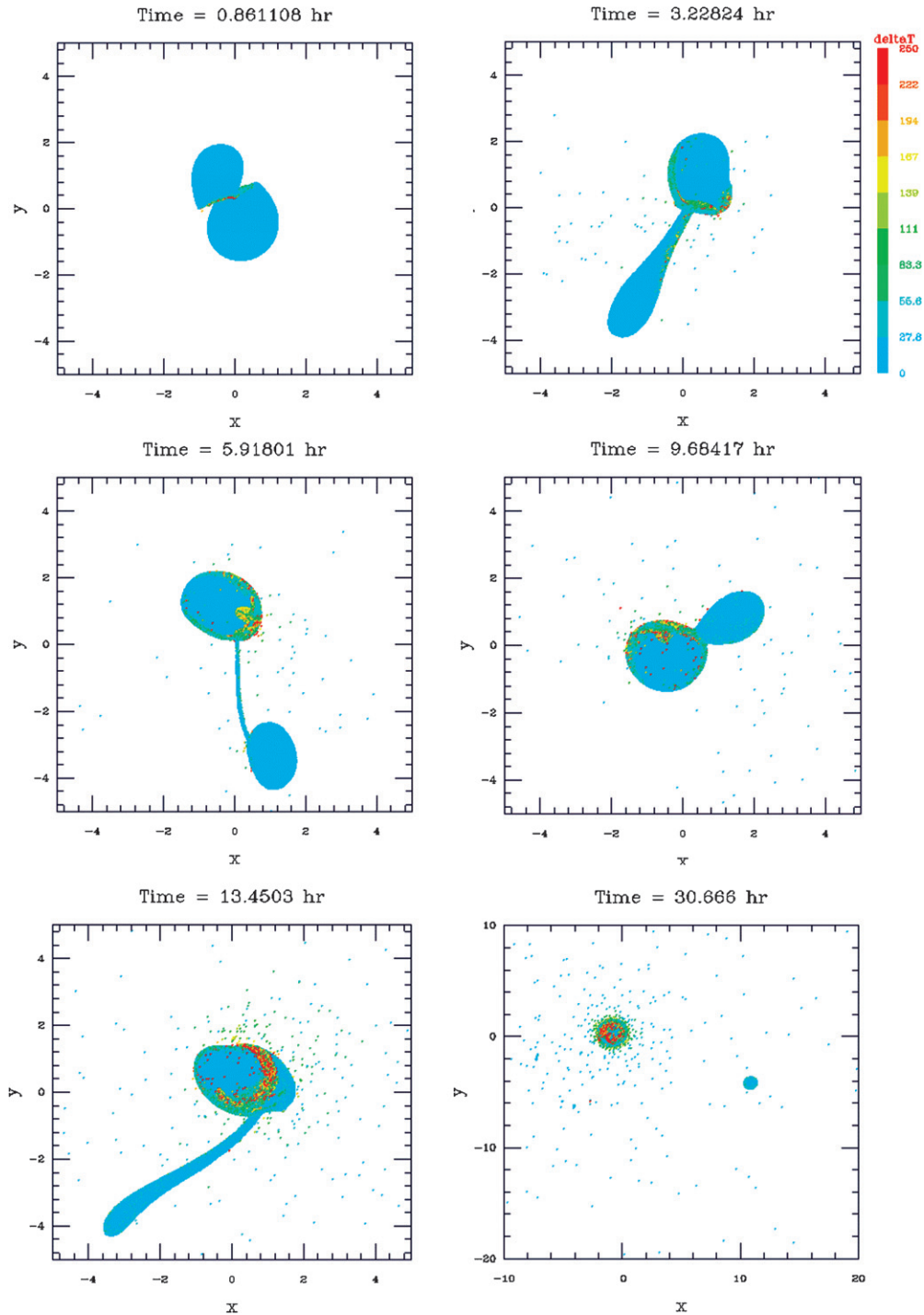


Figure 2. Million-particle SPH simulation of the grazing collision of two objects having a thin, pure ice shell (comprising 10% of each object’s total mass) overlying a hydrated silicate (serpentine) interior, a structure intended to represent a partially differentiated state. Other parameters of this collision are similar to those of the impact in Figure 1 (see the main text for details). Color scales with the temperature change as in Figure 1. Here the final intact satellite contains 8% of the planet’s mass, and it is accompanied by an orbiting disk of material that is predominantly ice. The final state of an intact moon and a disk is a promising condition for producing a Charon–Nix–Hydra-like system.

general, impact velocities in excess of $1.2v_{\text{esc}}$ lead to the escape of the impactor for relatively oblique collisions.

Figures 5 and 6 show results from all of the simulations that produced an intact moon together with a disk. Resulting moon-to-planet mass ratios (Figure 5(a)) fall into two distinct groupings: $q \sim 0.1$ and $q \sim 0.4$, with the latter corresponding to cases in which the impactor is essentially captured intact during the collision. A similarly broad range of initial orbital eccentricities and semimajor axes for the intact moons to that

found in Canup (2005) is found here (Figure 5(b)). While e and a vary substantially, the great majority of the intact moons have an initial periapse between and 3 and $4R_p$.

Figure 6 shows the mass and composition of the debris disk as a function of its maximum radial extent. For each disk particle, I calculate the radius of its equivalent circular orbit, a_{eq} . The maximum equivalent circular orbit for a disk particle, $a_{\text{eq,max}}$, ranges from just above the planet’s surface to nearly $30R_p$. The masses of the debris disks are generally much larger than the

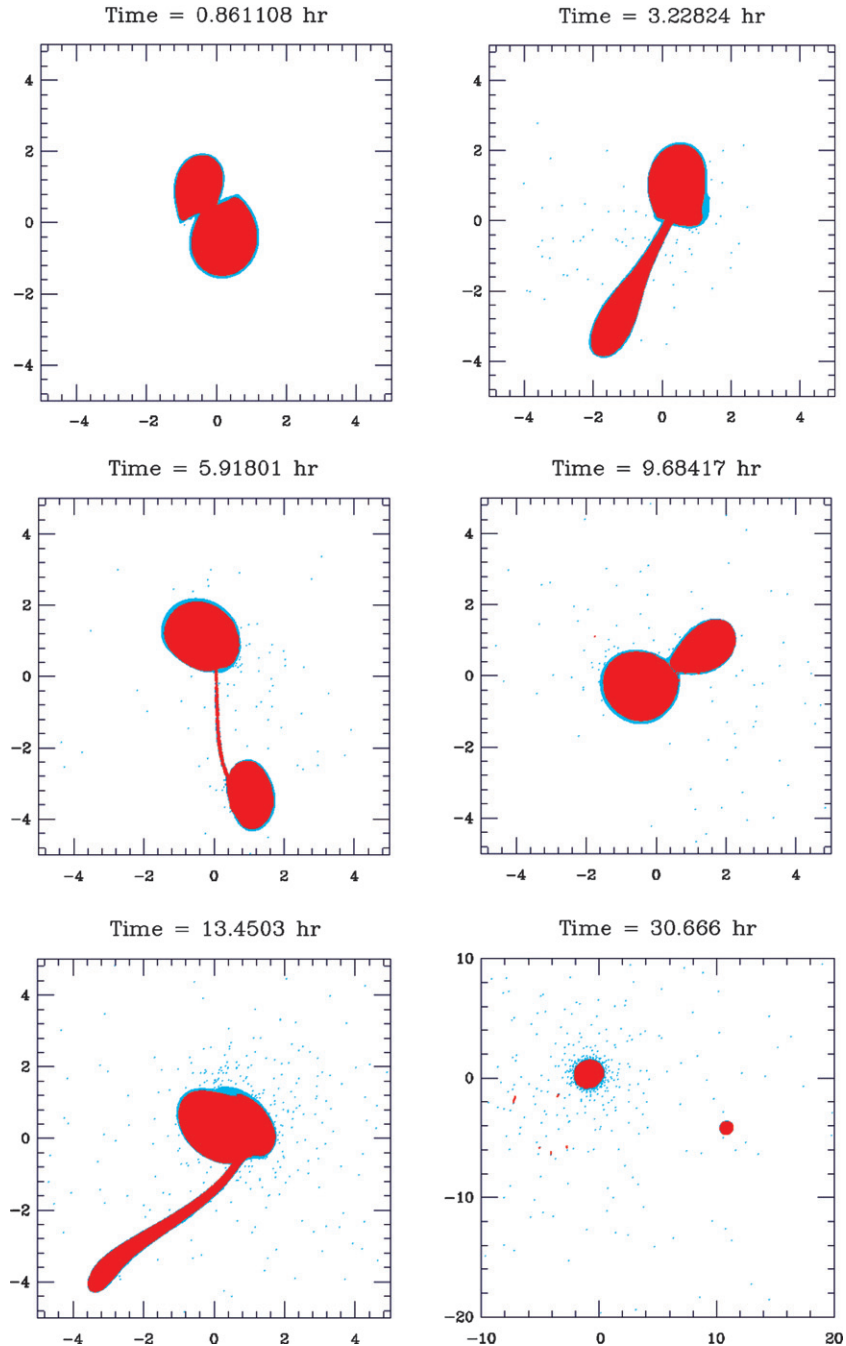


Figure 3. Same collision as shown in Figure 2, only here color indicates material type (red: hydrated silicate; blue: water ice).

estimated masses of Nix and Hydra (Figure 6(a)). Most of the disks are enhanced in ice compared to the starting composition of the colliding objects, which contained 15% (10%) ice by mass for the 10^5 -particle (10^6 -particle) simulations. In 40% of the intact moon-disk cases, the majority of the disk mass is ice (Figure 6(b)).

4. CONCLUSIONS AND IMPLICATIONS

It is possible to generate a planet-moon-disk system through a single giant impact that is broadly consistent with that needed to produce Pluto's system of three satellites. The successful impacts involve a low-velocity (with $v_{\text{imp}}/v_{\text{esc}} \leq 1.2$, or a velocity at infinity less than about 0.7 km s^{-1}), highly oblique ($b \geq 0.75$) collision between similarly sized objects that are

partially differentiated, containing a small fraction of their mass in an outer pure ice shell. Similar collisions involving uniform composition, undifferentiated objects typically lead to the formation of a single intact moon and no disk as found in Canup (2005), a result that appears unaffected by the factor of 50 increase in the number of SPH particles considered here (e.g., Figure 1). Similar collisions involving fully differentiated rock-ice objects that contain 40%–50% ice by mass form a disk, rather than a large intact satellite (Canup 2005). The disk in these cases is composed of ice, inconsistent with Charon's bulk density, which implies a substantial rock fraction.

In the impact scenario advocated here, Charon forms intact, with a density comparable to that of the bulk impactor and an initially eccentric orbit. It is accompanied by a debris disk that contains a similar or larger fraction of its mass in ice compared

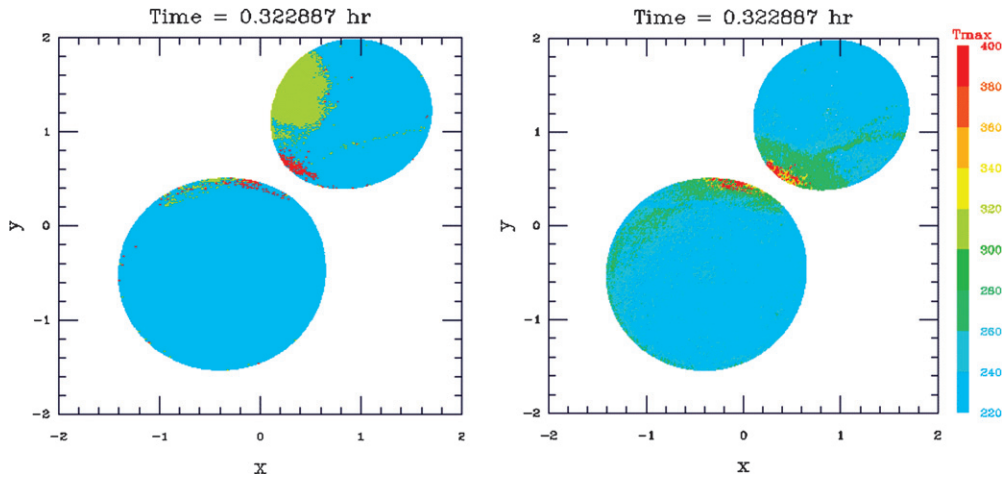


Figure 4. Mapping of particle quantities onto the figures of the impactor and target from a million-particle simulation (see the text for details) at a time just prior to the initial collision. Left panel: predicted final particle state at the end of the collision: escaping (red), bound in orbit about the final planet (yellow-green), or accreted by the planet (blue). Right panel: peak temperature experienced by each particle during the impact. The highest temperatures occur at the location of the initial grazing impact.

Table 2
Parameters and Outcomes of 10^5 -particle Impact Simulations^a

Run	γ	b	$v_{\text{imp}}/v_{\text{esc}}$	Impactor Spin Period (hr)	J	Outcome	q	a/R_p	e	M_d (g)
20	0.3	0.75	1.2	3	0.34	Moon + disk	0.081	4.57	0.18	2.30E+22
22	0.3	0.75	1.3	3	0.37	Impactor escapes
26	0.3	0.75	1.4	3	0.39	Impactor escapes
10	0.3	0.8	1.15	3	0.34	Moon + disk	0.088	4.65	0.14	3.10E+21
19	0.3	0.8	1.2	3	0.36	Moon + disk	0.389	10.4	0.87	1.30E+21
21	0.3	0.8	1.25	3	0.38	Impactor escapes
25	0.3	0.8	1.3	3	0.39	Impactor escapes
9	0.3	0.85	1.1	3	0.35	Moon + disk	0.086	5.28	0.26	1.20E+22
12	0.3	0.85	1.15	3	0.37	Moon + disk	0.408	9.93	0.86	7.30E+20
8	0.3	0.9	1.1	3	0.37	Moon + disk	0.408	8.16	0.82	3.20E+21
3	0.3	0.91	1.05	3	0.36	Moon + disk	0.083	7.44	0.47	3.00E+22
1	0.3	0.98	1	...	0.36	Moon + disk	0.088	15.8	0.77	5.00E+22
13	0.3	0.98	1	3	0.37	Moon + disk	0.101	13.02	0.73	2.60E+22
11	0.3	0.98	1.05	3	0.39	Moon	0.429	8.62	0.81	...
28	0.5	0.75	1.1	5	0.38	Moon + disk	0.067	25.74	0.88	5.80E+22
23	0.5	0.75	1.2	5	0.41	Disk	2.62E+23
18	0.5	0.8	1.1	5	0.40	Disk	3.21E+23
27	0.5	0.8	1.15	5	0.42	Disk	2.04E+23
5	0.5	0.85	1	5	0.39	Moon + disk	0.105	5.01	0.22	4.00E+21
17	0.5	0.85	1.05	5	0.41	Moon + disk	0.089	8.74	0.63	2.50E+22
6	0.5	0.85	1.1	5	0.43	Moon + disk	0.044	26	0.85	2.90E+23
7	0.5	0.89	1.05	5	0.43	Disk	4.51E+23
15	0.5	0.9	1.1	5	0.45	Moon + disk	0.053	26.4	0.86	3.30E+23
4	0.5	0.91	1	5	0.42	Moon + disk	0.163	4.15	0.11	6.00E+20
16	0.5	0.95	1	5	0.44	Moon + disk	0.124	5.5	0.33	1.50E+20
14	0.5	0.95	1.05	5	0.46	Moon + disk	0.149	5.92	0.44	2.20E+21

Notes.

^a See the text for definition of symbols. The final four columns list the moon-to-planet mass ratio, the moon's semimajor axis and eccentricity, and the mass of the debris disk. For comparison, the mass ratio of Charon to Pluto is $q = 0.12$, while the masses of Nix and Hydra are estimated to be $\sim \text{few} \times 10^{20}$ g each.

to the composition of the impactor. Some of the debris disks are found to be sufficiently radially extended to account for debris near or in the 4:1 and 6:1 resonances with a newly formed Charon (26% have $a_{\text{eq,max}} > 15R_p$ and 11% have $a_{\text{eq,max}} > 20R_p$), although most are less radially extended than this. This result should be considered somewhat uncertain. Even the highest resolution simulations can only barely resolve the small masses needed to account for Nix and Hydra. Higher resolution simulations than those currently feasible would be needed to

reach firm conclusions about the distribution of orbiting material at the $\sim 10^{20}$ g level.

However, it does appear clear that the debris disks are substantially more compact than the current orbits of Nix and Hydra, located at approximately 43 and 57 Pluto radii. Thus, formation of Nix and Hydra through a Charon-forming impact appears to require that the small satellites formed at much smaller orbital radii than their current positions and were subsequently driven outward, presumably by resonant

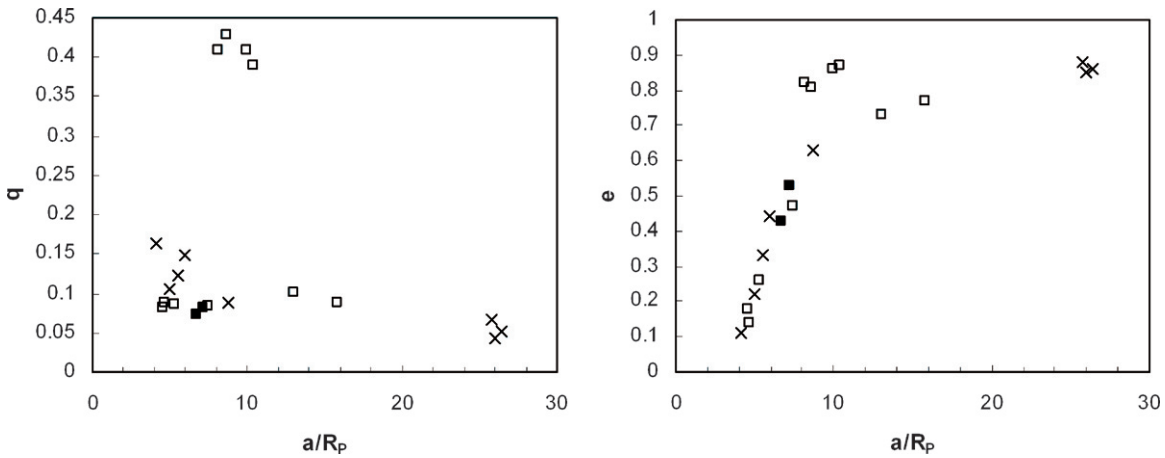


Figure 5. Intact moon properties from “successful” SPH simulations that produced a large intact moon together with a debris disk. Open squares and crosses correspond to $N = 10^5$ particle runs with $\gamma = 0.3$ and 0.5 , respectively. Filled squares are 10^6 -particle simulations with $\gamma = 0.3$. Left panel: moon-to-planet mass ratio, q , vs. the intact moon’s semimajor axis. Right panel: orbital eccentricity, e , and semimajor axis, a , of the intact moon’s orbit in units of the planet’s radius, R_p .

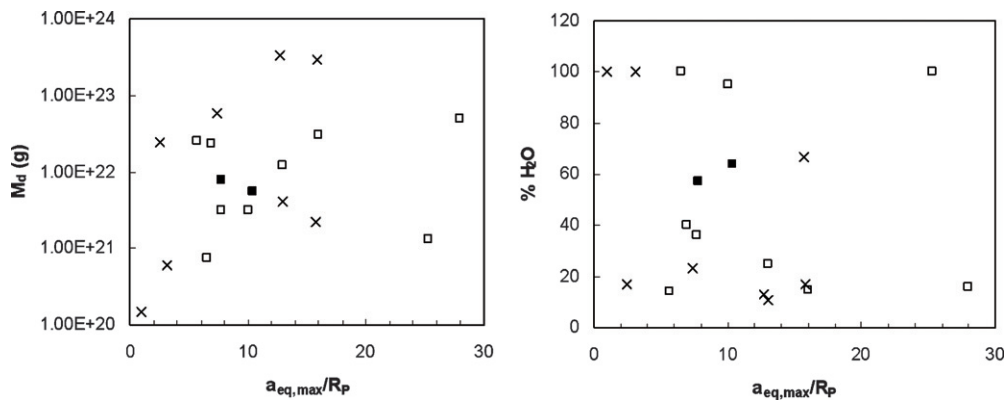


Figure 6. Disk properties from “successful” SPH simulations that produced a large intact moon together with a debris disk (see the caption to Figure 5 for definitions of symbols). Left panel: mass in debris disk vs. the maximum equivalent circular orbit of disk material ($a_{eq,max}$) scaled to the planet’s radius. Right panel: percentage of the disk’s mass in ice vs. $a_{eq,max}$.

interaction with Charon. The initial debris disks are predicted to be much more massive than needed to explain Nix and Hydra, although the disk masses are still small compared to Charon’s mass. It seems plausible that the great majority of orbiting disk material would have eventually been accreted by Charon, with only a very small fraction captured into resonances that would protect it from collision with Charon as the large satellite tidally evolved outward (e.g., Ward & Canup 2006).

How such a resonance expansion would proceed is still unclear. Planet and satellite tides could drive substantial changes in Charon’s e and a relative to those shown in Figure 5(b) on a timescale that is long compared to the SPH simulations, but short compared to Charon’s overall tidal evolution timescale. Thus, whether an orbital configuration exists that would allow for resonant transport of Nix and Hydra by Charon in recently proposed scenarios (e.g., Ward & Canup 2010) cannot be addressed by impact simulations alone.

Although I have focused on the origin of Nix and Hydra by impact, an alternative is that the small moons formed from material captured into Pluto’s orbit subsequent to the impact formation of Charon (e.g., Lithwick & Wu 2008). The results here suggest that if Nix and Hydra were produced by the Charon-forming impact, their composition would be similar to or more ice-rich than Charon and Pluto, and a pure ice composition for Nix and Hydra falls within the range of possible outcomes. In contrast, a capture origin would generally imply a solar composition mixture of rock and ice, leading to densities

comparable to those of Charon and Pluto. Thus if future observations find that Nix and Hydra have ice-like densities, this would argue for an impact origin, while a mixed ice–rock composition would be consistent with either an impact or a capture origin. Current observations suggest that if Nix and Hydra have ice-like densities, their albedos must be much lower than that of Charon (Tholen et al. 2008). Other models suggest that ejecta mixing within the Pluto system should lead to similar albedos in all three moons (Stern 2009), although this would lead to unrealistically high densities for the small moons given current estimates for their masses (Tholen et al. 2008). More detailed information on the properties of Nix and Hydra should be forthcoming through either stellar occultations and/or the *New Horizons* flyby in 2015.

This work was supported by the National Science Foundation’s Planetary Astronomy program. The author thanks David Kaufmann and Peter Tamblin for their help in developing and implementing the parallelized SPH code used here, and Amy Barr and William Ward for helpful comments on the paper.

REFERENCES

- Benz, W. 1989, in *Numerical Modeling of Nonlinear Stellar Pulsations, Problems and Prospects*, ed. J. R. Buchler (Dordrecht: Kluwer), 269
 Brown, M. E., et al. 2006, *ApJ*, **639**, 43
 Buie, M., Grundy, W. M., Young, E. F., Young, L. A., & Stern, S. A. 2006, *AJ*, **132**, 290
 Canup, R. M. 2004, *Icarus*, **168**, 433

- Canup, R. M. 2005, *Science*, 307, 546
- Canup, R. M. 2008, *Icarus*, 196, 518
- Canup, R. M., & Asphaug, E. 2001, *Nature*, 412, 708
- Canup, R. M., & Pierazzo, E. 2006, in 37th Annual Lunar and Planetary Science Conf. League City, TX, [Abstract No. 2146](#)
- Dobrovolskis, A. R., Peale, S. J., & Harris, A. W. 1997, in *Pluto and Charon*, ed. S. A. Stern & D. J. Tholen (Tucson, AZ: Univ. Arizona Press), 159
- Leinhardt, Z. M., Marcus, R. A., & Stewart, S. T. 2010, *ApJ*, 714, 1789
- Lithwick, Y., & Wu, Y. 2008, arXiv:0802.2951
- Lithwick, Y., & Wu, Y. 2010, preprint
- McKinnon, W. B. 1989, *ApJ*, 344, 41
- Melosh, H. J. 2007, *Meteorit. Planet. Sci.*, 42, 2079
- Nicholson, P. D., Čuk, M., Sheppard, S. S., Nesvorný, D., & Johnson, T. V. 2008, in *The Solar System Beyond Neptune*, ed. M. A. Barucci, H. Boehnhardt, D. P. Cruikshank, & A. Morbidelli (Tucson, AZ: Univ. Arizona Press), 411
- Olkin, C. B., Wasserman, L. H., & Franz, O. G. 2003, *Icarus*, 164, 254
- Peale, S., Lee, M. H., & Cheng, T. 2010, in 2010 Nix-Hydra Meeting, Baltimore, MD (<https://webcast.stsci.edu/webcast/detail.xhtml?sessionId=44F3A51510D982A8548B0ABB082ECDA0?talkid=1917&parent=1>)
- Stern, S. A. 2009, *Icarus*, 119, 571
- Stern, S. A., et al. 2006, *Nature*, 439, 946
- Tholen, D. J., Buie, M. W., Grundy, W. M., & Elliott, G. T. 2008, *AJ*, 135, 777
- Thompson, S. L., & Lauson, H. S. 1972, Technical Rep. SC-RR-710714 (Albuquerque, NM: Sandia Nat. Labs)
- Ward, W. R., & Canup, R. M. 2006, *Science*, 313, 1107
- Ward, W. R., & Canup, R. M. 2010, in 2010 Nix-Hydra Meeting, Baltimore, MD (<https://webcast.stsci.edu/webcast/detail.xhtml?sessionId=44F3A51510D982A8548B0ABB082ECDA0?talkid=1917&parent=1>)
- Weaver, H. A., et al. 2006, *Nature*, 439, 943